

The Eastern Pacific ITCZ during the Boreal Spring

GUOJUN GU

Goddard Earth Sciences and Technology Center, University of Maryland, Baltimore County, Baltimore, and Laboratory for Atmospheres, NASA Goddard Space Flight Center, Greenbelt, Maryland

ROBERT F. ADLER

Laboratory for Atmospheres, NASA Goddard Space Flight Center, Greenbelt, Maryland

ADAM H. SOBEL

Department of Applied Physics and Applied Mathematics, and Department of Earth and Environment Sciences, Columbia University, New York, New York

(Manuscript received 16 March 2004, in final form 19 June 2004)

ABSTRACT

The 6-yr (1998–2003) rainfall products from the Tropical Rainfall Measuring Mission (TRMM) are used to quantify the intertropical convergence zone (ITCZ) in the eastern Pacific (defined by longitudinal averages over 90°–130°W) during boreal spring (March–April). The double-ITCZ phenomenon, represented by the occurrence of two maxima with respect to latitude in monthly mean rainfall, is observed in most but not all of the years studied. The relative spatial locations of maxima in sea surface temperature (SST), rainfall, and surface pressure are examined. Interannual and weekly variability are characterized in SST, rainfall, surface convergence, total column water vapor, and cloud water. There appears to be a competition for rainfall between the two hemispheres during this season. When one of the two rainfall maxima is particularly strong, the other tends to be weak, with the total rainfall integrated over the two varying less than does the difference between the rainfall integrated over each separately. There is some evidence for a similar competition between the SST maxima in the two hemispheres, but this is more ambiguous, and there is evidence that some variations in the relative strengths of the two rainfall maxima may be independent of SST.

Using a 25-yr (1979–2003) monthly rainfall dataset from the Global Precipitation Climatology Project (GPCP), four distinct ITCZ types during March–April are defined, based on the relative strengths of rainfall peaks north and south of, and right over, the equator. Composite meridional profiles and spatial distributions of rainfall and SST are documented for each type. Consistent with previous studies, an equatorial cold tongue is essential to the existence of the double ITCZs. However, too strong a cold tongue may dampen either the southern or northern rainfall maximum, depending on the magnitude of SST north of the equator.

1. Introduction

Of the global tropical oceans, the eastern Pacific has perhaps the strongest annual cycle (e.g., Mitchell and Wallace 1992; Li and Philander 1996). Intense air–sea interactions in this region result in a cold equatorial zone (usually called the equatorial cold tongue)–intertropical convergence zone (ITCZ) complex during the boreal summer and fall. A narrow band of frequent deep convection (i.e., the ITCZ) appears between 5° and 10°N, associated with warm sea surface tempera-

ture (SST), while a large area of cold SST (<26°C) and infrequent deep convection occurs near to and south of the equator. During the boreal spring, two ITCZs, represented by monthly mean rainfall, are usually observed straddling the equator (Lietzke et al. 2001; Halpern and Hung 2001; Zhang 2001). This double ITCZ is coincident with the occurrence of relatively high SST (compared to immediately neighboring regions, or the same region at other times of year) along and south of the equator, and with seasonal weakening of southeasterly trade winds (e.g., Hayes et al. 1989; Kessler et al. 1998).

Using satellite-observed cloud data, Hubert et al. (1969) showed the presence of two convective zones in the eastern Pacific during March–May 1967. However, they concluded that the double ITCZ is not a charac-

Corresponding author address: Guojun Gu, Code 912, Goddard Space Flight Center, Greenbelt, MD 20771.
E-mail: ggu@agnes.gsfc.nasa.gov

teristic feature of the tropical circulation. Recent satellite observations have improved our knowledge of this phenomenon. General agreement seems to have been reached that a double ITCZ normally occurs in the eastern Pacific during the boreal spring (Zheng et al. 1997; Lietzke et al. 2001; Halpern and Hung 2001; Zhang 2001). Moreover, a recent study of high-resolution surface wind observations from the spaceborne scatterometer QuikScat found that the double ITCZ is discernible year-round in the Atlantic and eastern Pacific Oceans, if it is defined by using the surface convergence field rather than precipitation (Liu and Xie 2002). Liu and Xie (2002) used a short data record (fully covering only two episodes of the double ITCZs), and focused on surface wind; they did not include data for related fields, such as rainfall and water vapor. Lietzke et al. (2001) described temporal (weekly and monthly) and spatial patterns of several ITCZ-related variables during boreal spring in the eastern Pacific using the Special Sensor Microwave Temperature Profiler (SSM/T)-2-derived cloud and water vapor, the Microwave Sounding Unit (MSU)-derived rainfall, and the *European Remote Sensing Satellite (ERS)-1* and -2 scatterometer wind field. Their study was primarily concentrated on the 3 yr of 1995–97.

With the availability of six-season (1998–2003) high-quality satellite rainfall observations from the Tropical Rainfall Measuring Mission (TRMM), the first objective of this study is to characterize the spatial and temporal variation of convection and rainfall in the eastern Pacific during boreal spring, with a specific interest in the occurrence of the double ITCZs. Compared to Lietzke et al. (2001) and Liu and Xie (2002), we use different and longer-record satellite observations, including six-season TRMM-measured rainfall, and TRMM Microwave Imager (TMI)-measured cloud, water vapor, and SST. The year-to-year variation of the double ITCZs is emphasized, and shorter time-scale evolution within each year is also examined.

Our second objective is to describe the observed relationships between the different variables studied here. Specifically, we wish to clarify what kind of meridional profiles of SST is generally preferred by the double ITCZs (defined here by precipitation, rather than surface convergence, unless stated otherwise), and to document the relative positions of maxima in the different variables. These issues are relevant for validating (or defining errors in) double ITCZs that are simulated in general circulation models, and perhaps also for testing theories for the mechanisms by which SST controls deep convection.

Details of the datasets are described in section 2. In section 3, the relationship among tropical deep convection, SST, and surface wind fields on monthly and weekly time scales are examined using the 6-yr (1998–2003) TRMM rainfall products, 6-yr (1998–2003) TMI SST estimates, and 4-yr (2000–03) QuikScat wind fields, respectively. Based on the previous conclusion that the

double ITCZs are primarily observed in March and April (e.g., Lietzke et al. 2001; Zhang 2001), our monthly analysis will be concentrated on these months. The associations between rainfall and SST are further investigated in section 4 by means of a 25-yr (1979–2003) rainfall product from the Global Precipitation Climatology Project (GPCP) and the 22-yr (1982–2003) Reynolds SST (Reynolds et al. 2002). Finally, conclusions and implications of the study are given in section 5.

2. Data

TRMM products 3B43 (monthly) and 3B42 (daily) are used to describe the ITCZ-related convection and rainfall. In particular, the monthly mean product (3B43) is used to define the ITCZ in this study. These two datasets are produced by using (nearly) coincident TRMM Combined Instrument (TCI) [the combined algorithm using both the TMI and TRMM precipitation radar (PR)] and Visible Infrared Scanner (VIRS) data, to calibrate the geoinfrared (IR) rain rate (Adler et al. 2000). This strategy provides much better rain-rate estimates than simple fixed-calibration geo-IR estimates, but with the same superior time sampling as the latter. The datasets are archived on a 1° latitude \times 1° longitude grid, and extend from January 1998 to the present.

The monthly and weekly TMI SST data used here are retrieved from the TMI on board the TRMM satellite. TMI can measure SST in the presence of overlying cloud, if the cloud is not precipitating. This is a distinct advantage over IR estimates, which require a cloud-free field of view (Wentz and Schabel 2000). The data cover a global region extending from 40°S to 40°N at a spatial resolution of 0.25° (detailed algorithms can be found in Wentz 1997). TMI-derived cloud liquid water and column water vapor data are also used; they have the same spatial coverage and resolution as the TMI-measured SST.

Surface wind fields are obtained from the SeaWinds scatterometer on board the QuikScat satellite (Liu et al. 1998; Liu and Xie 2002). Because the measurements became available only after July 1999, monthly and weekly products from January 2000 to May 2003 are used, extending from 90°S to 90°N , with a spatial resolution of 0.25° .

A long-record (1979–2003) monthly mean rainfall dataset from GPCP is used to confirm the results from the TRMM rainfall products and to provide a preliminary climatology of the ITCZ during the boreal spring. On a global $2.5^\circ \times 2.5^\circ$ grid, the data are combined from various information sources (Adler et al. 2003): the IR rainfall estimates are from geostationary and polar-orbiting satellites, the microwave estimates are from Special Sensor Microwave Imager (SSM/I) data, and surface gauge data are from the Global Precipitation Climatological Center (GPCC). For this climatology, the monthly mean SST of Reynolds et al. (2002), archived on $1^\circ \times 1^\circ$ grids for the years 1982–2003, was used.

3. TRMM years (1998–2003)

a. Monthly mean

Figure 1 shows the monthly mean rainfall and SST in boreal spring averaged over the six TRMM years (1998–2003). Two distinct rainfall maxima appear on either side of the equator from the central to eastern Pacific during March–April. As was found in previous studies, the double ITCZ appears to be a regular feature within the large-scale annual cycle in the eastern Pacific. In February and May, two rainfall peaks can also be seen, but the southern peak is mostly west of 130°W and perhaps should be associated with the South Pacific convergence zone (SPCZ).

The spatial distribution of surface rainfall generally follows that of the SST. The equatorial cold tongue becomes weak during March–April, but is still discernible. North of the equator, the ITCZ gradually strengthens from February to May, concomitant with a steady SST increase. South of the equator, the SST attains its highest values in March and April in the eastern Pacific (east of about 130°W). It seems that the occurrence of the southern rainfall peak is favored by a weak but discernible equatorial cold tongue and warmer SST (>27°C) south of the equator, which is generally consistent with results from previous studies (e.g., Lietzke et al. 2001; Zhang 2001).

1) RAINFALL, SST, AND SURFACE PRESSURE

Relationships between rainfall, SST, and surface pressure [from the National Centers for Environmental Prediction (NCEP)–National Center for Atmospheric Research (NCAR) reanalysis project (Kalnay et al. 1996), subject to the influence of the numerical model involved in the data assimilation and, therefore, subject to question more than the other observed fields] are further examined comparing their respective meridional profiles for each individual year (Figs. 2 and 3). Inspection of Fig. 1 shows that the longitude range (90°–150°W) used in Lietzke et al. (2001) actually includes, at different longitudes, two distinct SST maxima south of the equator. In the western portion, closer to 150°W, the latitudinal SST maximum is further south and is quite distinct from that further east. Although the rainfall maximum is continuous, we consider the western SST maximum to be associated with the SPCZ, which is distinct from the eastern Pacific ITCZ. Here, we thus focus on averages that are only over the eastern ITCZ, defined here as the region between 90° and 130°W.

In 1998, warm equatorial SST and off-equatorial SST maxima (>28°C between 10°S and 10°N) occur in both March and April without any significant SST minimum along the equator. In that year, the intense rainfall band is broad and extends continuously from 5°S to 5°N, though a northern peak does appear in March. This is

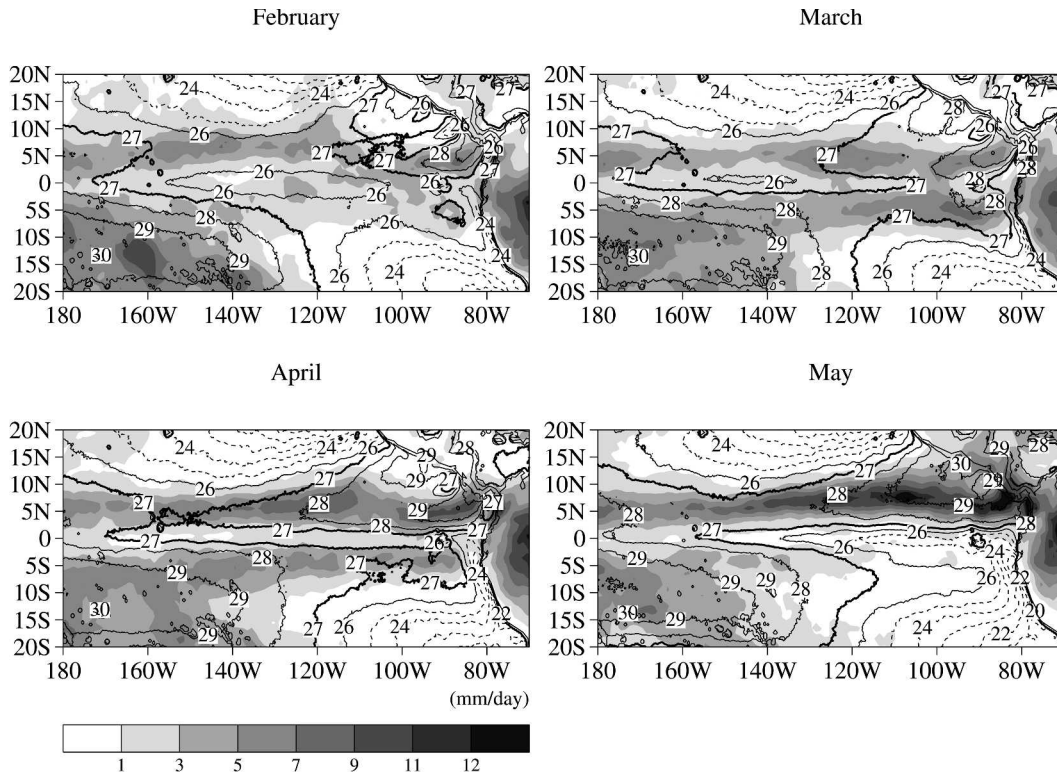


FIG. 1. Monthly TRMM rainfall (mm day⁻¹; shaded) and TMI SST (°C; contours) averaged over the six TRMM years (1998–2003) in the tropical Pacific ocean during boreal spring.

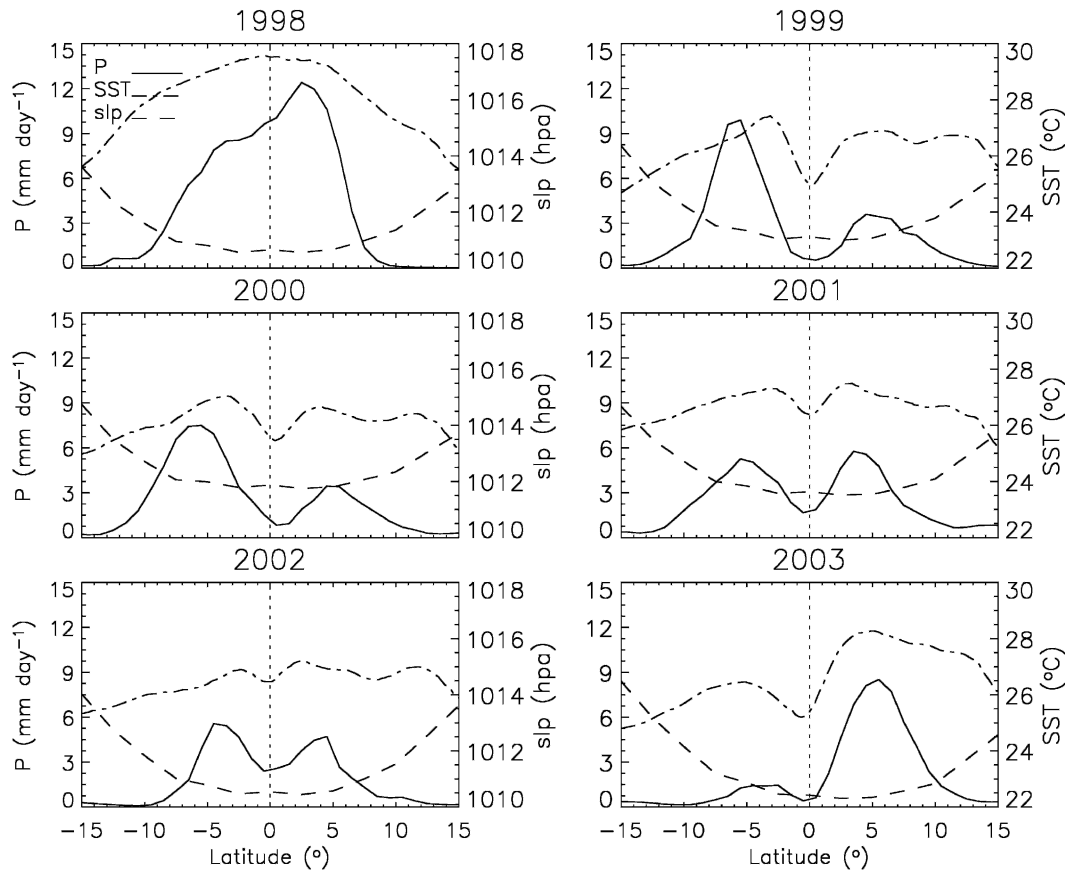


FIG. 2. Meridional profiles of monthly TRMM rainfall [P (mm day^{-1}); solid lines], sea level pressure [slp (hPa); dashed lines], and TMI SST ($^{\circ}\text{C}$; dash-dot lines) between 90° – 130°W in Mar.

consistent with the notion that the double ITCZ tends not to occur during the El Niño events because of the disappearance of the equatorial cold tongue (e.g., Zhang 2001).

In almost all of the months shown, the surface pressure has a very broad minimum centered approximately at the equator, with essentially a zero gradient between approximately 5°S and 5°N . In some cases there is a slight hint of a very weak local maximum within that minimum, right on the equator.

In the four double-ITCZ years (i.e., 1999, 2000, 2001, and 2002), local SST maxima appear on both sides of the equator, separated by a minimum on the equator. Particularly in March, the southern SST peaks are at least comparable in magnitude to their northern counterparts. The equatorial cold tongue in these 4 years is considerably weaker than in 2003, according to the difference between the equatorial SST and off-equatorial SST maxima. In the double-ITCZ years, the rainfall peaks in March are generally found a few degrees of latitude poleward of the SST peaks, whereas the two tend to be collocated in April. In 1998 and 2003, the rainfall peaks are roughly collocated with the SST maxima. These findings are systematically different

from Lietzke et al. (2001). They found that the rainfall maxima tend to be equatorward of the SST maxima. We have computed meridional profiles of TRMM rainfall and TMI SST between about 90° and 150°W (not shown); these are somewhat different from the 90° – 130°W results because of the impact of the SPCZ. However, similar discrepancies between these results and those of Lietzke et al. (2001) can still be seen, suggesting that these discrepancies result, to a significant extent, from the different datasets used.

Tomas and Webster (1997) stated that SST and rainfall maxima tend to be collocated when the cross-equatorial surface pressure gradient is weak, and displaced more from one another when it is strong. Considering all of the months shown in Figs. 2 and 3, the relative displacement of the SST and precipitation maxima ranges from 0° to perhaps 5° at most, which in all cases is significantly less than the distance between the two ITCZs. To the extent that this qualifies as a “small” displacement, these results appear consistent with the findings of Tomas and Webster (1997). Such displacements that do occur tend to place the rainfall maxima systematically poleward of the SST maxima. Tomas and Webster (1997) also stated that rainfall

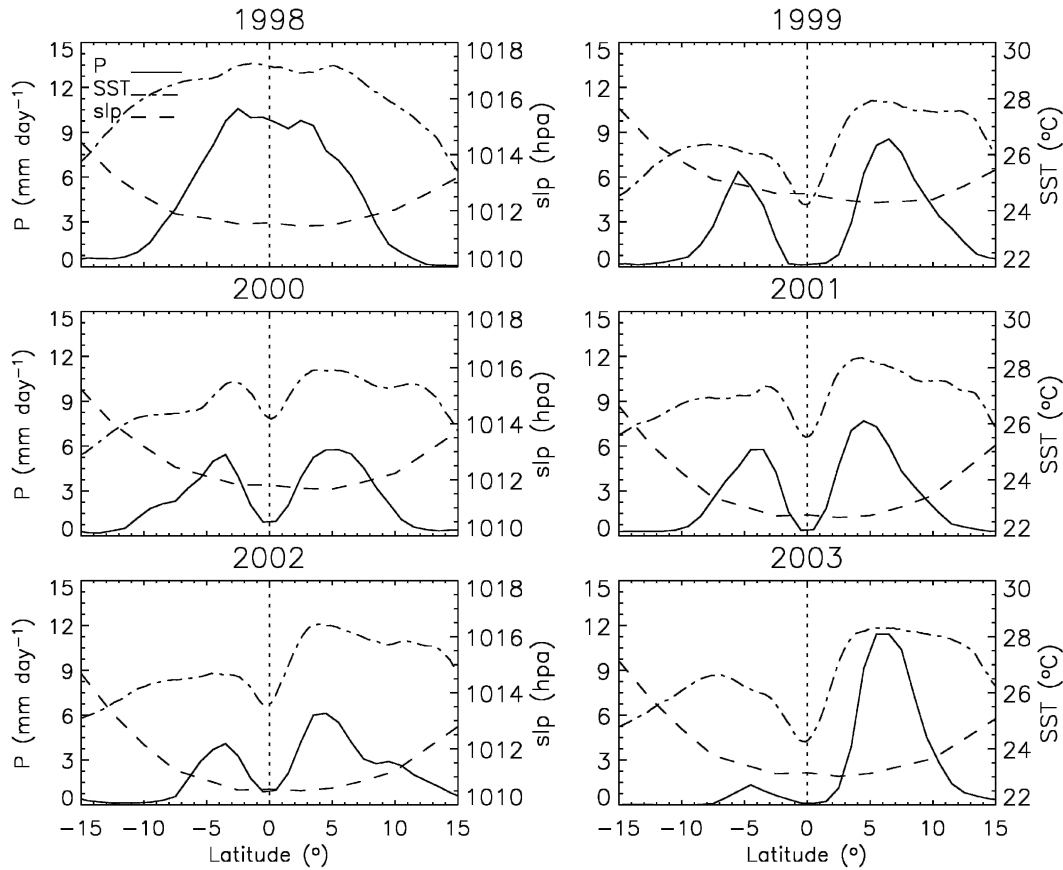


FIG. 3. Same as in Fig. 2, but in Apr.

maxima tend to lay equatorward of surface pressure troughs. Unusual in other ways, the eastern Pacific double ITCZs in boreal spring are clearly an exception to this general rule as well. Although the pressure troughs are so broad in Figs. 2 and 3 that it is hard to pinpoint the absolute minima with precision, in most cases—April 1998 being the clearest counterexample—the precipitation maximum lies either distinctly poleward of the pressure minimum, or at least near the poleward edge of the region of near-zero gradient.

2) COMPETITION BETWEEN THE TWO ITCZs

Inspection of Figs. 2 and 3 leads to the impression that, from year to year and month to month (within boreal spring), there is a competition between the northern and southern ITCZ (as measured by rainfall), with an approximate conservation of the total rainfall integrated over both. In other words, when one ITCZ is particularly strong the other is weak, and when both are of a comparable magnitude that magnitude is less than the magnitude of the stronger one at those (other) times in which one dominates. The strong El Niño year, 1998, is again the exception to this.

This is made more quantitative by Figs. 4a and 4b. To

produce this figure, we first compute the total integrated rainfall over the northern and southern ITCZs, P_{NH} and P_{SH} , respectively. These are defined by integrals from 0° to $15^\circ N$ and 0° to $15^\circ S$, respectively. We then plot the sum, $P_{NH} + P_{SH}$, as a function of the difference $|P_{NH} - P_{SH}|$ in a scatterplot, where each point is one of the months shown in Figs. 2 and 3. Figure 4a does this from the TRMM data. Excluding 1998 (crosses nearest to the upper-left corner), we see that the range of variation in the sum, which is the total rainfall over both ITCZs together, is smaller than the range of variation in the difference. Figure 4b shows the same thing, but is computed from the longer-record GPCP data. In this case, again excluding the El Niño years (crosses), the scatter is somewhat larger, and there is a slightly larger linear trend (indicating a tendency toward more total rainfall when the northern ITCZ is stronger than the southern), but qualitatively, the result is similar to Fig. 4a. These results quantify the notion in the previous paragraph that there is an apparent competition between the two ITCZs, with approximate conservation of the total rainfall in both together. The situation may be compared to that of a single convective zone whose location shifts from month to month or year to year, while its intensity

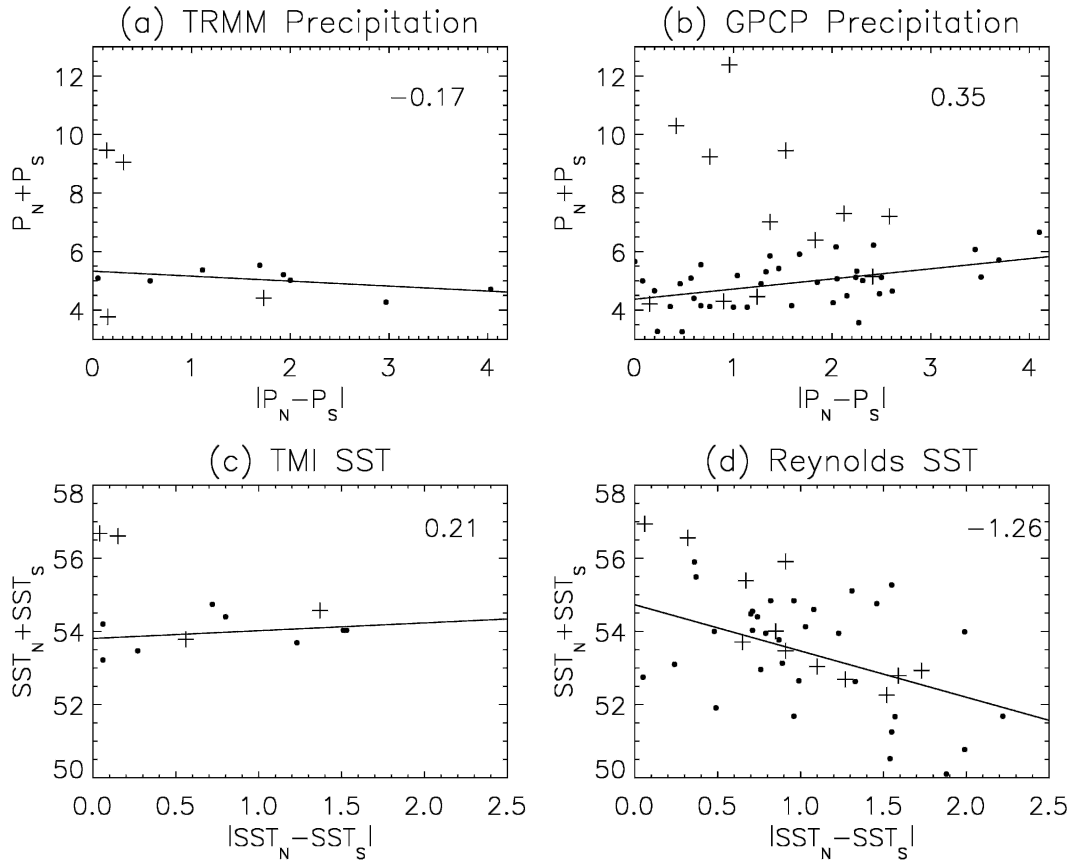


FIG. 4. (a), (b) $P_{NH} + P_{SH}$ vs $|P_{NH} - P_{SH}|$; P_{NH} and P_{SH} are domain mean monthly rainfall in Mar and Apr; P_{NH} is averaged between 0° and 15°N , 90° and 130°W ; P_{SH} is averaged between 0° and 15°S , 90° and 130°W . (c), (d) $SST_{NH} + SST_{SH}$ vs $|SST_{NH} - SST_{SH}|$; SST_{NH} and SST_{SH} are domain mean SST in Mar and Apr. SST_{NH} is averaged between 0° and 15°N , 90° and 130°W ; SST_{SH} is averaged between 0° and 15°S , 90° and 130°W . Dots are for the non-El Niño years, and crosses are El Niño years. The linear trends are only for the non-El Niño years. The units of precipitation and SST are mm day^{-1} and $^\circ\text{C}$, respectively.

changes relatively little; the difference here is that, with El Niños excluded, the rainfall skips the equator and rather is “exchanged” between two relatively fixed locations at a finite distance from one another. This result might be expected, to the extent that we expect the overall supply of moisture from the larger trade winds regions feeding the ITCZs to be relatively constant. Even if that is assumed, however, it might still be possible for the eastern Pacific ITCZ to exchange moisture in a more interannually variable way with regions to its east or west.

It is natural to ask how much of this result is due to coupled interaction, and how much is due to internal atmospheric dynamics. For example, Hack et al. (1989) suggested that a stronger northern ITCZ may suppress the southern one through large-scale subsidence, a mechanism that could operate independently of SST, echoing arguments made earlier by Graham and Barnett (1987). On the other hand, if the competition between the two ITCZs is due to coupled interaction (or, for that matter, ocean processes alone, which would

then influence the atmosphere through their effect on SST), we would expect to see a competition in SST similar to that seen in precipitation. In that case, the precipitation signal could be viewed as an essentially deterministic response to SST. In Figs. 4c and 4d, we define SST_{NH} and SST_{SH} to be exactly analogous to P_{NH} and P_{SH} , making the same plots as in Figs. 4a and 4b. Figures 4c and 4d show the TMI and Reynolds SST, respectively. In Fig. 4c, we see that the TMI SST does show a competition similar to that seen in precipitation, with a warmer sea surface in one hemisphere that tends to be associated with a cooler one in the other, such that the SST integrated over both hemispheres changes relatively little. The Reynolds SST in Fig. 4d does not corroborate the competition, having much greater variations in $SST_{NH} + SST_{SH}$, and both scatter and a decreasing trend with increasing $|SST_{NH} - SST_{SH}|$. During the TRMM years (1998–2003), the Reynolds SST did show a seemingly similar, but much more scattered, pattern as that of the TMI-measured SST (not shown), probably suggesting discrepancies between these two

datasets. Comparing Figs. 4b and 4d shows, based on the longer datasets, that although total integrated SST is lower when the northern SST maximum exceeds the southern one by a larger margin, the total integrated rainfall has a slight tendency to increase in that circumstance. This may be counterintuitive to the extent that we expect rainfall and SST to be correlated, but actually this relationship applies usefully only to deviations from the larger-scale mean. In means over the entire Tropics, for example, SST and rainfall are at most very weakly correlated (Su and Neelin 2003).

We are, thus, left with a somewhat ambiguous result. Although the TMI SST data seem to indicate that the competition in precipitation is the deterministic result of a similar competition in SST, the TMI record is relatively short compared to the Reynolds data, which give a different answer. Even in the TMI data, we can find evidence for a nondeterministic component of the precipitation. The TMI SST profiles shown in Fig. 3 are nearly identical in April 1999 and 2003, while the associated rainfall profiles are very different, with a strong southern rainfall maximum in 1999 and almost none in 2003. Either precipitation is exquisitely sensitive to very

small SST differences, or this is a fairly dramatic example of the lack of an entirely deterministic, instantaneous relationship between rainfall and SST—at least on a monthly mean basis. The SST profiles differed more in March of those 2 years, with a significantly greater value in the northern maximum than the southern one in 2003, and a slightly greater value in the southern maximum than the northern one in 1999. Perhaps some atmospheric memory of the suppressed southern ITCZ (and strong northern one) is able to persist from March to April in 2003, despite the southern SST increase. For example, the water vapor field might carry such a memory, with descent during March 2003, leading to a relatively dry troposphere persisting into April [as is seen to some degree in section 3a(3)], which could suppress precipitation. To further explore the possible nondeterministic component of precipitation, scatterplots of rainfall, SST, and surface convergence [more results and discussions about surface convergence are in section 3a(4)] are shown at three different latitudinal belts (Fig. 5): 5°S, 0°, and 5°N. Such scatterplots should be regarded with some care, particularly when the data span interannual or longer time

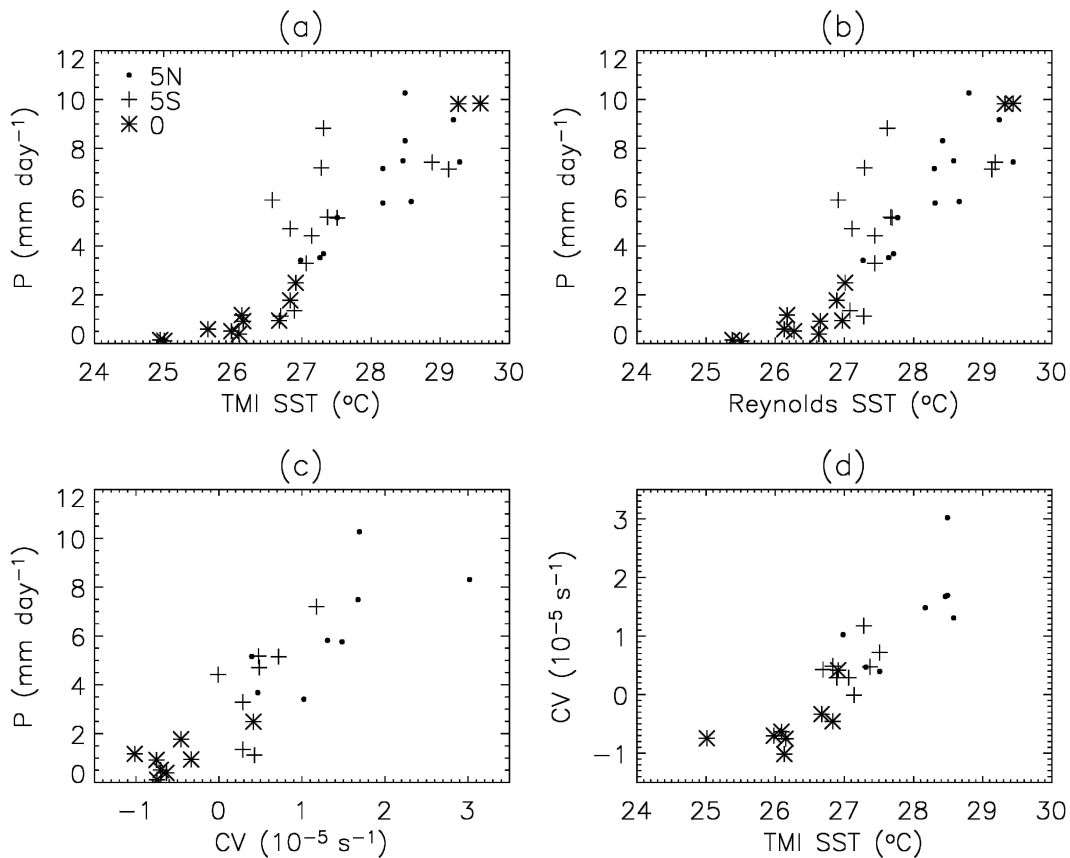


FIG. 5. (a) TRMM precipitation (mm day⁻¹) vs TMI SST (°C), (b) TRMM precipitation (mm day⁻¹) vs Reynolds SST (°C), (c) TRMM precipitation (mm day⁻¹) vs QuikScat surface convergence (10⁻⁵ s⁻¹), and (d) QuikScat surface convergence (10⁻⁵ s⁻¹) vs TMI SST (°C) at 5°S (crosses), 0° (stars), and 5°N (dots) during Mar–Apr; (a) and (b) are from 1998 to 2003; (c) and (d) are from 2000 to 2003.

scales. On these time scales the tropical mean SST and the mean tropospheric temperature generally vary, particularly with ENSO (Hurrell and Trenberth 1998; Wentz and Schabel 2000; Soden 2000; Sobel et al. 2002). We generally expect rainfall to be locally related not to the absolute SST, but to the difference between the local SST and the larger-scale mean (Neelin et al. 2003). Nonetheless, somewhat compact relationships can be found among the variables shown in Fig. 5. However, along 5°S—roughly the location of the southern ITCZ—only weak correlations seem to exist between rainfall and SST, and to some degree between rainfall and surface convergence, which is different than the correlations over the equator and along 5°N. Also, at a given value of rainfall, the points along 5°S tend to lie systematically at lower values of SST than those at 5°N. It seems that a lower SST at 5°S accompanies the same amount of rainfall as that at 5°N, further emphasizing the role of internal atmospheric dynamics. A simple, theoretically possible explanation might be that there is more boundary layer moisture at 5°S than at 5°N, but that seems relatively unlikely because the SST is generally lower in the southern than the northern maximum,

and we expect relative humidity in the planetary boundary layer to be fairly tightly constrained in the Tropics (e.g., Held and Soden 2000), so that SST and boundary layer specific humidity will tend to be tightly coupled.

3) RAINFALL, CLOUD LIQUID WATER, AND WATER VAPOR

Monthly mean profiles of TMI column water vapor and cloud liquid water are illustrated in Figs. 6 and 7 for comparison to surface rainfall. The peaks of these three variables are generally collocated. During the months when a southern ITCZ is well defined, water vapor and cloud liquid water have similar regional maxima in the Southern Hemisphere, though differences in the two fields' structure can be readily found at a finer level of detail. Column water vapor is much more smoothly distributed across the equator than the other two variables. In March 1998 one broad water vapor peak is observed right over the equator, whereas rainfall and clouds have sharper maxima at the latitude of about 2°–3°N. Local maxima in cloud liquid water need not always be accompanied by comparably strong rainfall peaks, for instance, south of the equator in 2003. Simi-

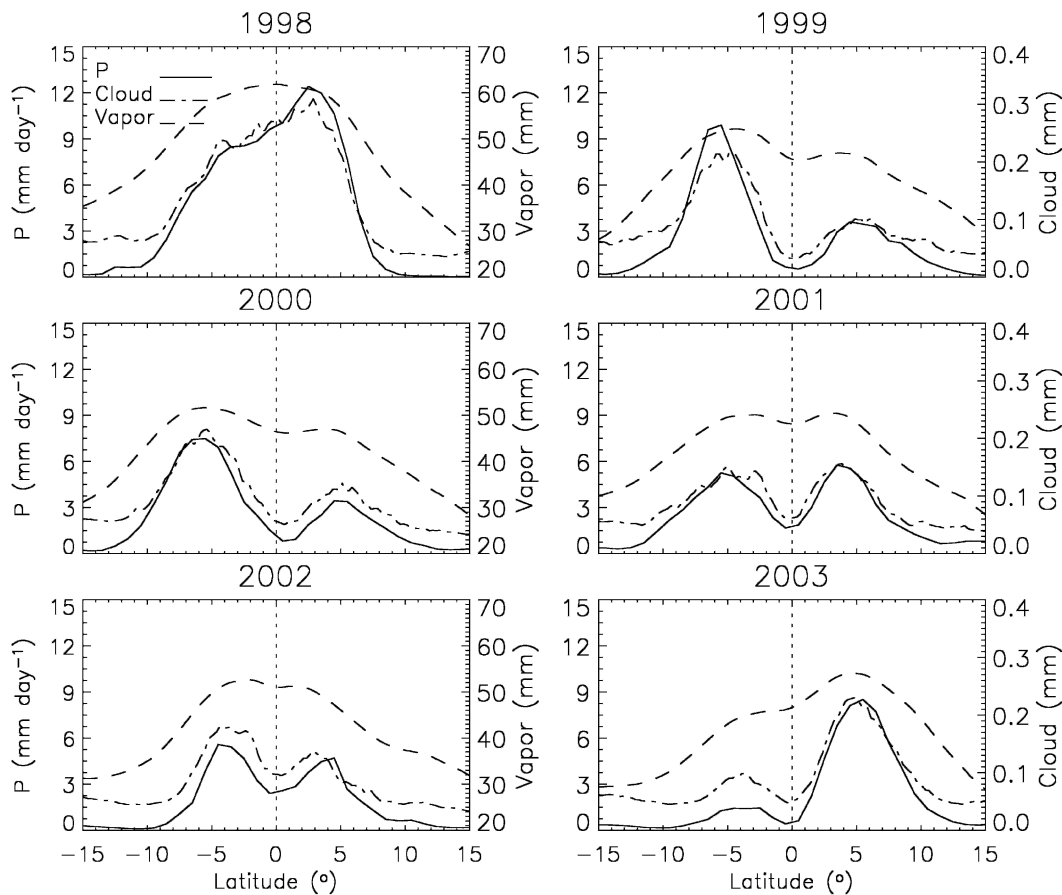


FIG. 6. Meridional profiles of monthly TRMM rainfall [P (mm day^{-1}); solid lines], TMI cloud liquid water (mm ; dash-dot lines), and TMI columnar water vapor (mm ; dashed lines) between 90° and 130°W in Mar.

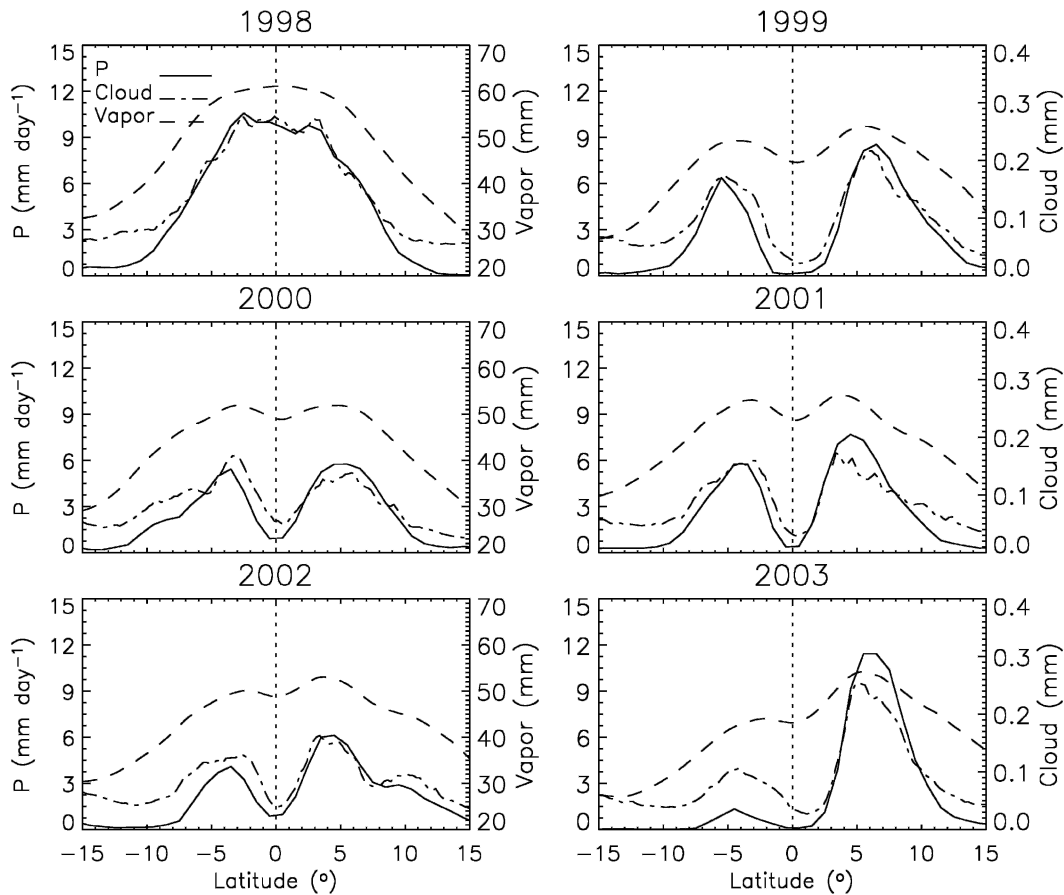


FIG. 7. Same as in Fig. 6, but in Apr.

larly, a certain amount of cloud liquid water is always observed south (north) of about 10°S (10°N), whereas no significant rainfall occurs there. This cloud liquid water is probably related to low-level stratocumulus clouds over relatively colder waters (e.g., Philander et al. 1996). Over somewhat warmer waters, there is presumably some signal from trade cumulus or midlevel weakly precipitating or nonprecipitating cumulus congestus (e.g., Johnson et al. 1999).

4) RAINFALL AND CONVERGENCE

We examine here the spatial relationships between surface convergence field and rainfall, taking advantage of the availability of the four-season (2000–2003) high-quality QuikScat surface wind product. The surface convergence (CV) field is estimated as $\text{CV} = -\nabla \cdot \mathbf{V} = -(\partial u/\partial x + \partial v/\partial y)$, here $\mathbf{V} = (u, v)$.

Meridional profiles of surface convergence and rainfall in March and April are shown in Fig. 8. Two convergence peaks are observed straddling the equator, concomitant with a divergence or weaker convergence (i.e., in March 2002) zone near the equator. The convergence in the Southern Hemisphere is at least com-

parable to its northern counterpart in March, with the exception of 2003. The spatial structures of the rainfall and convergence fields show salient differences. Rainfall peaks are not always located within the most intense convergence areas. The convergence maxima tend to be somewhat closer to the equator than the rainfall maxima, particularly in the Southern Hemisphere, with the convergence maxima roughly matching those in the SST (Figs. 2 and 3).

b. Weekly variation

Weekly rainfall averaged from the TRMM daily product (3B42) and weekly TMI-measured SST in the eastern Pacific during the boreal spring is shown in Fig. 9. Generally speaking, significant rainfall appears when and where SST is over $26^{\circ}\text{--}27^{\circ}\text{C}$ (e.g., Gadgil et al. 1984; Graham and Barnett 1987; Fu et al. 1990). This eastern Pacific threshold value is slightly lower than that found in the western Pacific and Indian Oceans, as found earlier by Fu et al. (1990). The most intense rainfall events were observed in 1998, during which time heavy precipitation fell without (spatial) interruption across the equator, which was extensively covered by warm water ($>28^{\circ}\text{C}$) due to the strong El Niño. In

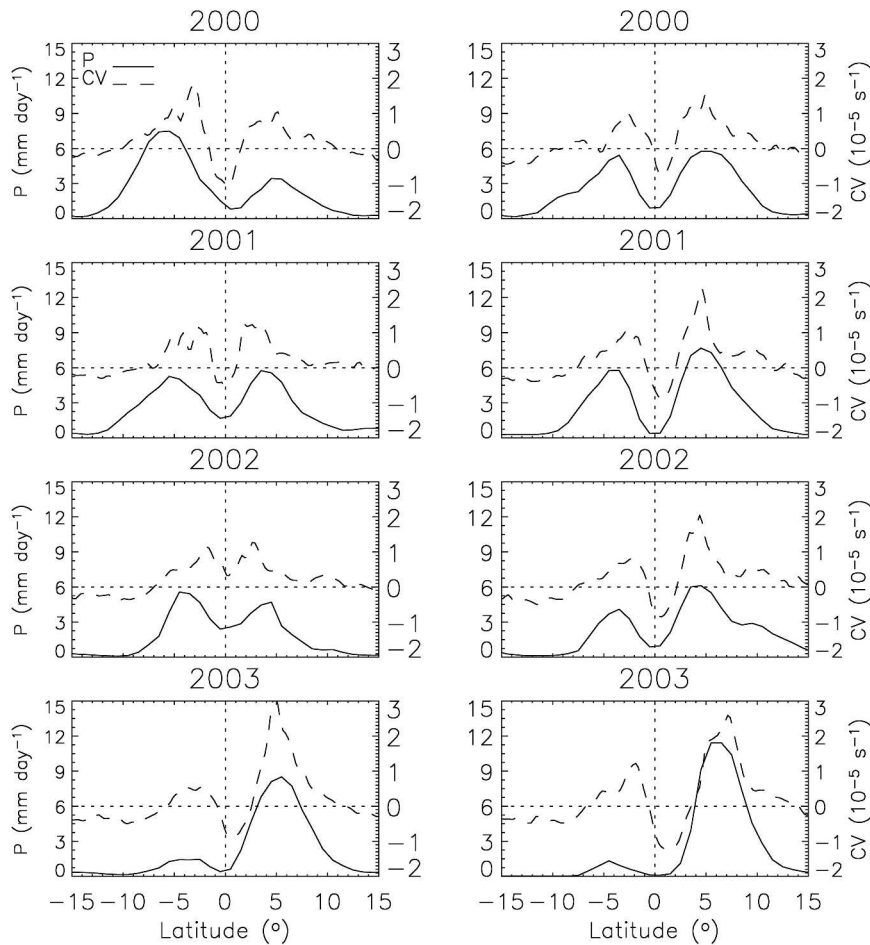


FIG. 8. Meridional profiles of monthly TRMM rainfall [P (mm day^{-1}); solid lines] and QuikScat surface convergence [CV (10^{-5} s^{-1}); dashed lines] between 90° and 130°W in (left) Mar and (right) Apr.

1999, 2000, 2001, and 2002 (the four double-ITCZ years), warmer SSTs (over 26°C) extended to the Southern Hemisphere, and, thus, the equatorial cold tongue became weaker during approximately days 60–130. Concurrently, the major rainfall zones shifted south of the equator. If a time mean meridional rainfall profile is calculated between day 60 and 100, the northern ITCZ is barely discernible in 1999 and 2000 (see Fig. 2). In contrast, rainfall events south of the equator are negligible in 2003, though a relatively warm water area can still be observed along 5°S roughly from day 60 to 140.

As in Figs. 2 and 3, but now at a weekly time scale, we see that surface rainfall does not exactly follow SST, though it is often close to doing so. Particularly in the four double-ITCZ years, major rainfall events south of the equator tend to occur along the southern boundary of the regions of greatest SST. After about day 120–130, the southern SST begins to drop, and the corresponding rainfall band, thus, disappears. Simultaneously, the northern ITCZ becomes significantly strengthened.

The weekly surface convergence field is also shown, using the weekly QuikScat wind vectors for the boreal spring during 2000–03 (Fig. 10). Two bands of surface convergence are evident during the entire time period (day 8–148), with a divergence zone meandering over the equator, consistent with Liu and Xie (2002). These two bands of convergence are not always associated with significant rainfall. The major rainfall events south of the equator only occur approximately during day 60–130 in 2000, 2001, and 2002. In 2003, no significant rainfall appears south of the equator, though there is still a salient (if somewhat weaker than in the other years) southern convergence zone. In the absence of deep convection and associated deep large-scale ascent in 2003, presumably the mass ascending out of the boundary layer is diverging again only slightly higher up, in a shallow circulation of the type recently documented in this region by Zhang et al. (2004).

Weekly TMI cloud liquid water and column water vapor are depicted in Figs. 11 and 12, respectively. Surface rainfall bands are marked by the simultaneous

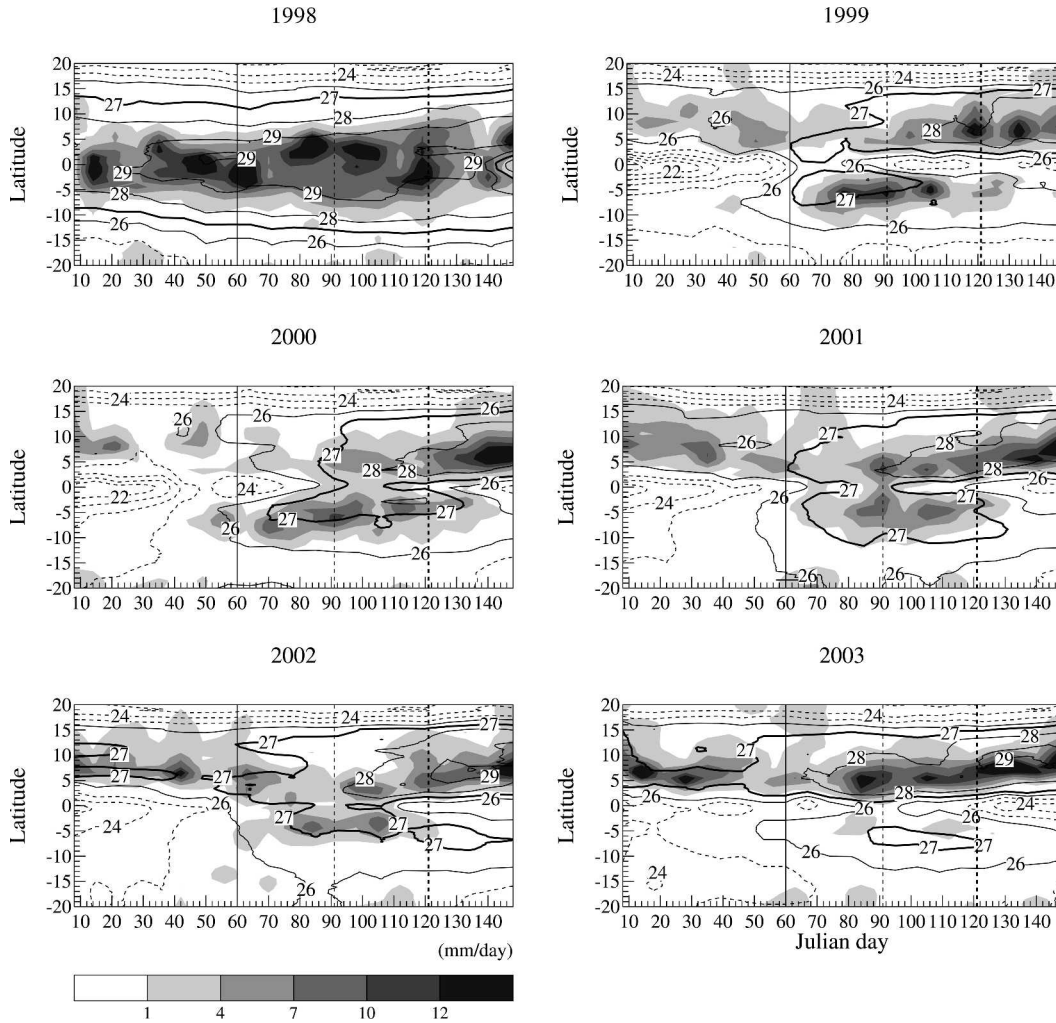


FIG. 9. Latitude–time diagram of weekly TRMM rainfall (mm day^{-1} ; shaded) and TMI SST ($^{\circ}\text{C}$; contours) averaged between 90° and 130°W : Thin solid, dashed, and thick dashed vertical lines denote 1 Mar (thin solid line), 1 Apr (dashed line), and 1 May (thick dashed line).

presence of clouds and regional water vapor peaks. There seems to be essentially no phase lag between rainfall and water vapor, consistent with a recent study that found the typical lag to be less than a day, which is too short to be visible in Figs. 11 and 12 (Bretherton et al. 2004). Major rainfall events south of the equator in the double-ITCZ years are concurrent with the southward (cross equatorial) excursion of high column water vapor values and the appearance of significant cloud activity. However, as noted above, there are several cases in which cloud liquid water peaks and regional water vapor maxima are not accompanied by any significant rainfall. In 2003, there are three consecutively occurring regional maxima of cloud liquid water and water vapor south of equator, without much rainfall. It is possible that this lack of deep convection is caused dynamically by enhanced subsidence associated with the intense northern convective band. As is shown in

Figs. 6 and 7, low-level stratocumulus clouds are widely seen south (north) of 10°S (10°N).

4. Climatological mean

Using the 25-yr (1979–2003) GPCP product, monthly mean rainfall, averaged between 90° and 130°W , is calculated during February–May for each year (dots in Fig. 13). The 25-yr mean meridional profiles of rainfall are also shown in Fig. 13. Two rainfall peaks occur in March and April, showing the climatological characteristics of the double ITCZs, in spite of strong interannual variability. In February and May, only a single ITCZ appears north of the equator. These features are generally in agreement with the currently archived TRMM observations (Figs. 1, 2, and 3).

For comparison, the mean meridional profiles of

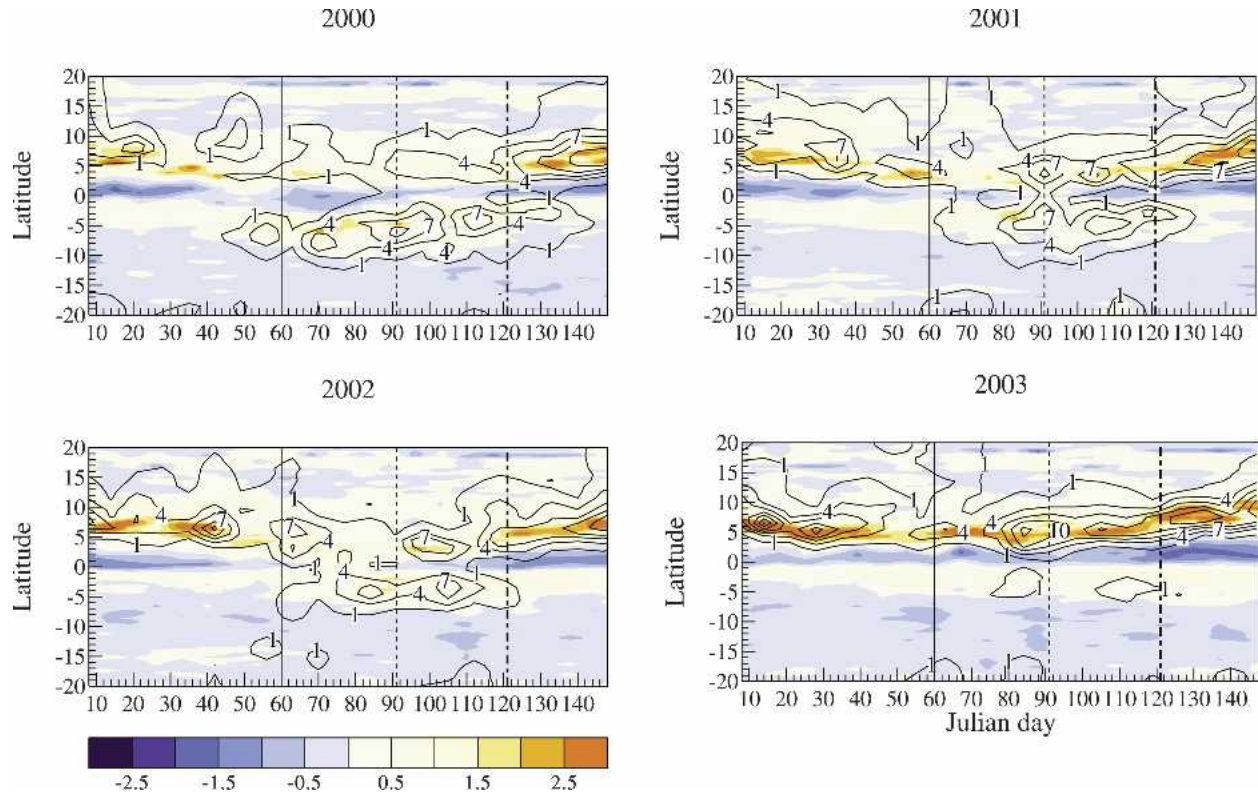


FIG. 10. Latitude–time diagram of weekly mean QuikScat surface convergence [$\text{CV} (10^{-5} \text{ s}^{-1})$; color shades] and TRMM rainfall (mm day^{-1} ; contours) between 90° and 130°W .

monthly rainfall data from the NCEP–NCAR reanalysis project are also shown (dashed lines in Fig. 13). The locations of the rainfall maxima from the NCEP–NCAR reanalysis project generally agree with those from the GPCP data, though a one gridpoint (2.5°) difference is found in several cases. In March and April, the magnitudes of the reanalysis rainfall peaks are similar to those of the GPCP. In May, the reanalysis data underestimate the northern rainfall peak but overestimate the southern one, compared to the GPCP data. The southern peaks in February and May suggest that erroneous double ITCZs exist in the reanalysis data. Presumably, this may be related to the influence of a numerical model on the reanalyzes in this data-sparse region. The tendency to produce a double ITCZ where and when one does not exist in reality is a well-known feature of many numerical models (e.g., Mechoso et al. 1995).

Based on the relative intensity of rainfall peaks south (P_{SH}) and north (P_{NH}) of the equator, and rainfall intensity over the equator (P_{eq}) during March–April (Fig. 13), we define four distinct ITCZ types (Table 1). The months corresponding to these ITCZ types are listed in Table 2. It shows that these four ITCZ types cover all of the possible configurations of the boreal spring ITCZ in the eastern Pacific.

Composite meridional profiles of monthly rainfall

are shown in Fig. 14a. Two major categories can be found: the double-ITCZ cases (type I) and the non-double-ITCZ cases (types II, III, and IV). Type II generally represents El Niño events. Intense rainfall covers the equatorial belt in these cases, although there is often still a rainfall peak in the Northern Hemisphere (dashed line in Fig. 14a). For types III and IV, in contrast, a single significant rainfall maximum is located either south or north of the equator. Furthermore, type III can only be found in March.

Composite meridional profiles of SST between 90° and 130°W are depicted in Fig. 14b, corresponding to the ITCZ types. As is shown by the TRMM observations (Figs. 2 and 3), higher SST is generally accompanied by greater rainfall. With a negligible equatorial cold tongue, the highest equatorial SST appears across the equator for type II, with a strong SST peak between 0° and 5°N , followed by intense mean rainfall. For the other three types, an equatorial cold tongue shapes two SST maxima. The intensities of the rainfall maxima do not exactly follow those of the SST maxima. In the Southern Hemisphere, the SST profiles look very similar, and the SST maxima are comparable in magnitude for these three non–El Niño types, in contrast to the large rainfall differences. Although, again, it is the contrast between the SST maximum and the SST of the rest of the Tropics (or at least the surrounding re-

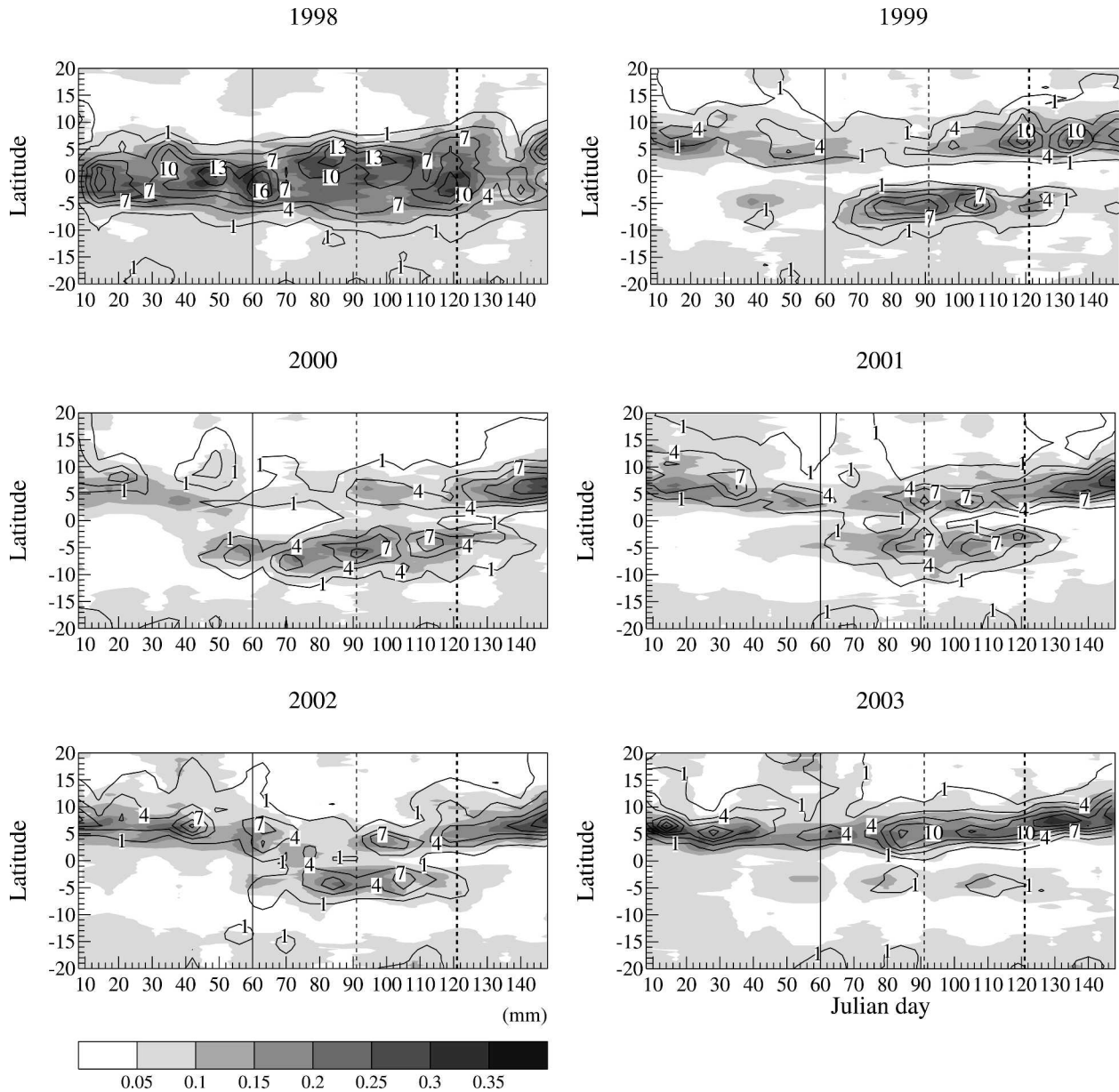


FIG. 11. Latitude–time diagram of weekly TRMM rainfall (mm day^{-1} ; contours) and TMI cloud liquid water (mm ; shaded) between 90° and 130°W .

gions) that we expect to be important; the tropical mean SST primarily tracks ENSO indices, such as Niño-3 (Sobel et al. 2002). Thus, the result just described, if it is real and not an artifact of the datasets, presumably indicates again that some monthly mean rainfall variations can be induced by atmospheric dynamics independently of SST. Furthermore, it seems that except in El Niño years, a stronger rainfall peak south of the equator tends to be more poleward of the SST maximum, which is qualitatively consistent with Figs. 2 and 3.

Composite horizontal distributions of rainfall and

SST are further displayed in Fig. 15. The type-II ITCZ generally reflects the impact of the equatorial warming during El Niño events. The type-I ITCZ shows two convective zones across the equator, roughly following the spatial distributions of SST. For type III, mean convection and rainfall are very weak north of the equator, particularly east of 120°W , but are strong south of the equator. In contrast, the mean rainfall for type IV is extremely strong in the Northern Hemisphere, while in the southern ITCZ it is negligible. Further, comparing the SST patterns for these three non-El Niño types, we see that the SST does not show large variations south of

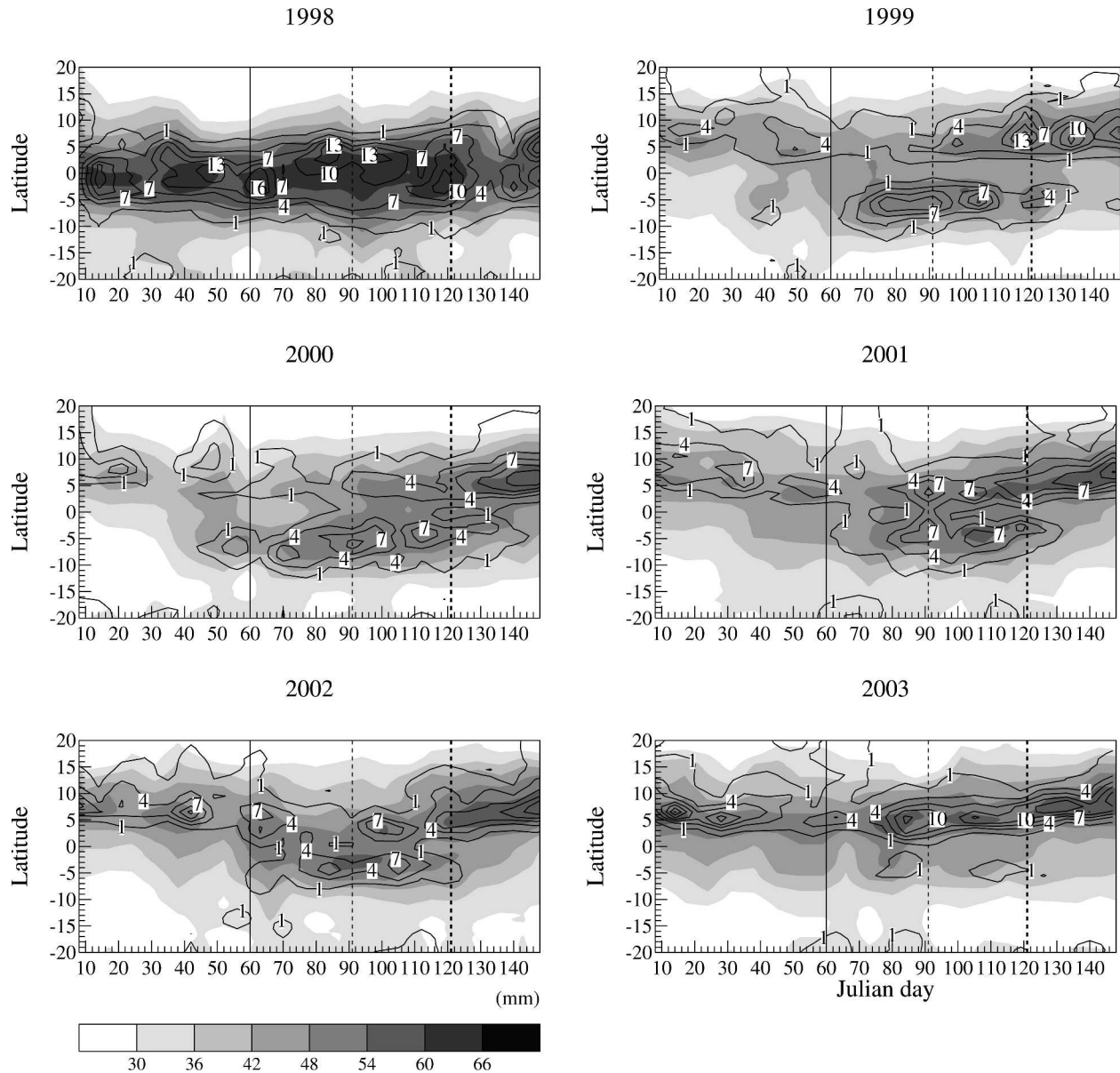


FIG. 12. Latitude–time diagram of weekly TRMM rainfall (mm day^{-1} ; contours) and TMI columnar water vapor (mm ; shades) between 90° and 130°W .

the equator, as shown in Fig. 14. Large SST differences are observed in the regions over the equator and north of the equator. Compared with the double-ITCZ type (type I), type III is accompanied by a colder equatorial region and much colder waters north of the equator, both of which are unfavorable for the northern ITCZ. For type IV, however, SST is very warm north of the equator, and the equatorial cold tongue is relatively weak (compared with type III), which tends to enhance (suppress) the northern (southern) ITCZ. It seems that the appearance and strength of the southern ITCZ is determined not only by the southern SST, but also by the SST over and north of the equator. This is consis-

tent with the competition mechanism suggested in the preceding section.

Lietzke et al. (2001) composited the meridional structures of rainfall and SST, and further proposed three types of atmospheric structures related to the eastern Pacific ITCZs during the boreal spring. Their classification was also based on the meridional distributions of SST, as follows: (a) a symmetric meridional SST with an equatorial cold tongue during the La Niña years, forcing two equally strong ITCZs; (b) an asymmetric meridional SST with an equatorial cold tongue and a stronger northern SST peak during the neutral years, forcing a stronger northern ITCZ and a weaker

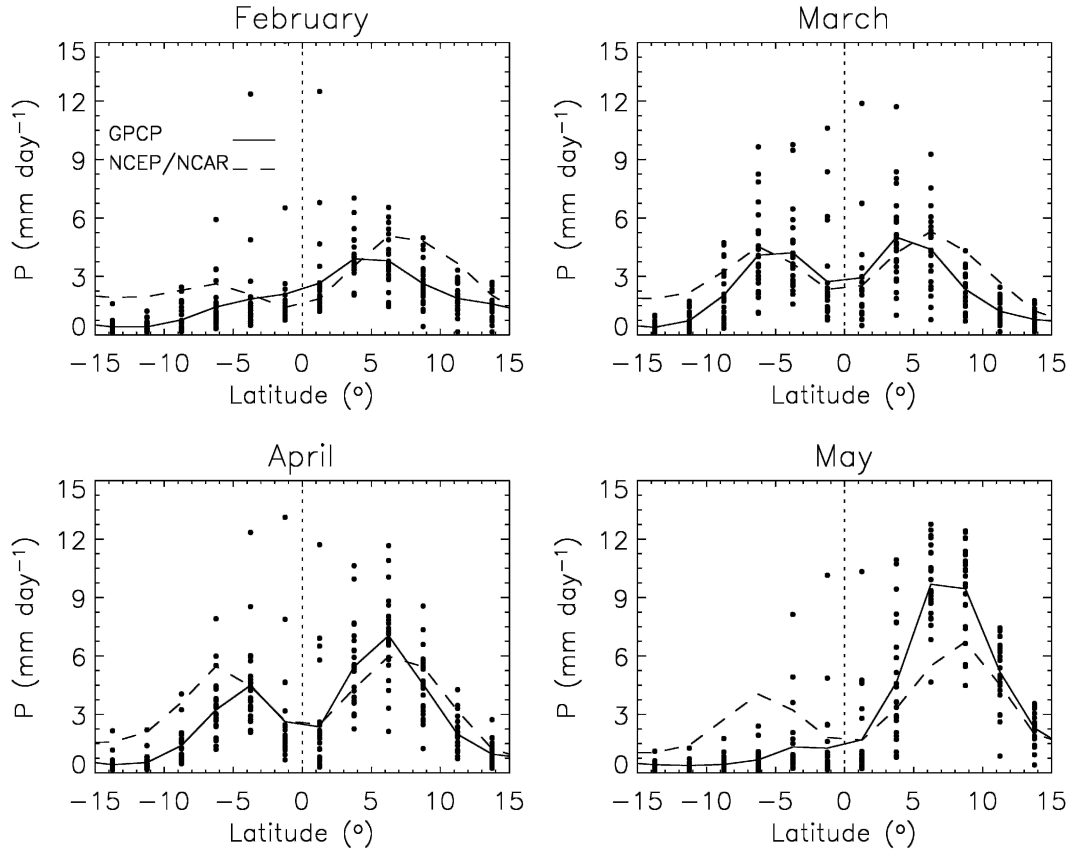


FIG. 13. Meridional profiles of monthly rainfall from GPCP (solid lines) and NCEP-NCAR reanalysis project (dashed lines) [P (mm day^{-1}); 90° and 130°W] during 1979–2003. Dots denote monthly GPCP rainfall in each year.

southern one; and (c) a broad, warm equatorial SST during El Niño years with one individual strong convective band covering the equatorial region. They ascribed the occurrence of a double ITCZ to an equatorial cold tongue. The results shown here are generally consistent with theirs. However, we subdivide the non-double ITCZ years further into types II, III, and IV, which correspond to three distinct spatial distributions of rainfall and SST. Particularly, we emphasize the existence of type III, though it appears only in March and only in a small number of years.

5. Summary and concluding remarks

The eastern Pacific ITCZ during boreal spring is quantified by the six-season TRMM rainfall data. Two

individual convective bands are observed straddling the equator during March and April in 1999, 2000, 2001, and 2002. The southern ITCZ becomes stronger than its northern counterpart in some cases. At times, deep convection can even shift entirely into the Southern Hemisphere for as much as several weeks. In the strong El Niño year of 1998, only one broad convective zone appears, and falls right across the equator. In 2003, one intense convective band is located around 5°N .

The ITCZs, as quantified by rainfall maxima, generally are closely associated in both space and time with

TABLE 1. The criterion used to define the ITCZ types during Mar–Apr. The unit of P_{eq} , P_{nh} , and P_{sh} is mm day^{-1} .

Type I (double ITCZ)	(i) $P_{\text{eq}} < 3$, (ii) $P_{\text{sh}}, P_{\text{nh}} \geq 3$ or $P_{\text{nh}} \geq 2, P_{\text{sh}} \leq 5$
Type II (El Niño)	$P_{\text{eq}} \geq 3$
Type III (south dominant)	(i) $P_{\text{eq}} < 3$, (ii) $P_{\text{sh}} \geq 3$, if $P_{\text{nh}} < 2$ or $P_{\text{sh}} > 5$, if $2 \leq P_{\text{nh}} < 3$
Type IV (north dominant)	(i) $P_{\text{eq}} < 3$, (ii) $P_{\text{nh}} \geq 3$, if $P_{\text{sh}} < 2$ or $P_{\text{nh}} > 5$, if $2 \leq P_{\text{sh}} < 3$

TABLE 2. The years categorized by the ITCZ types during Mar–Apr.

	Mar	Apr
Type I	1979, 1982, 1984, 1986, 1988, 1990, 1993, 1994, 2001	1979, 1980, 1982, 1984, 1985, 1986, 1988, 1989, 1991, 1993, 1994, 1996, 1999, 2000, 2001, 2002
Type II	1983, 1987, 1992, 1997, 1998, 2002	1983, 1987, 1992, 1998
Type III	1985, 1989, 1996, 1999, 2000	
Type IV	1980, 1981, 1991, 1995, 2003	1981, 1990, 1995, 1997, 2003

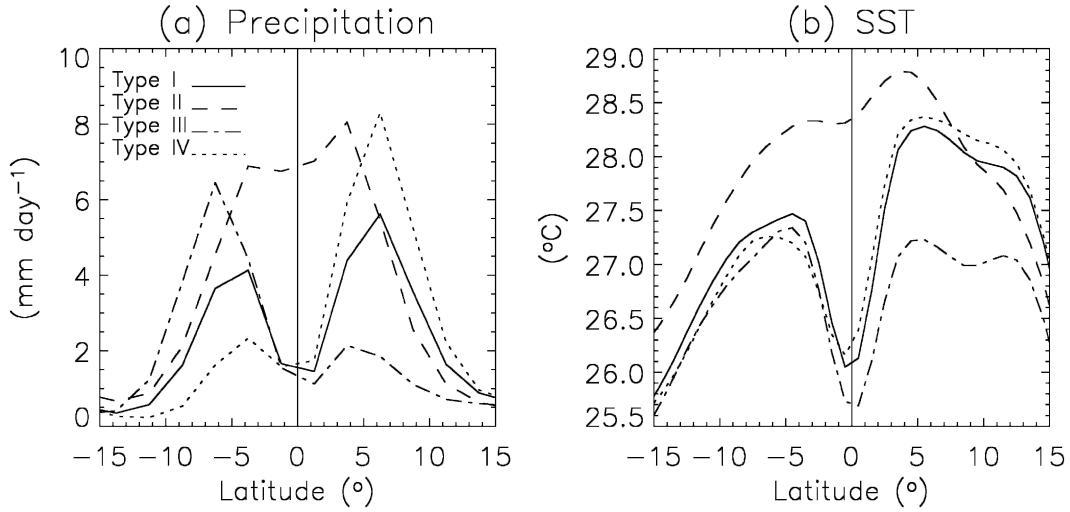


FIG. 14. Composite meridional profiles of monthly (a) GPCP rainfall (mm day^{-1}) and (b) Reynolds SST ($^{\circ}\text{C}$) between 90° and 130°W for the four ITCZ types during Mar–Apr. Type I (solid lines), type II (dashed lines), type III (dash-dotted lines), and type IV (dotted lines).

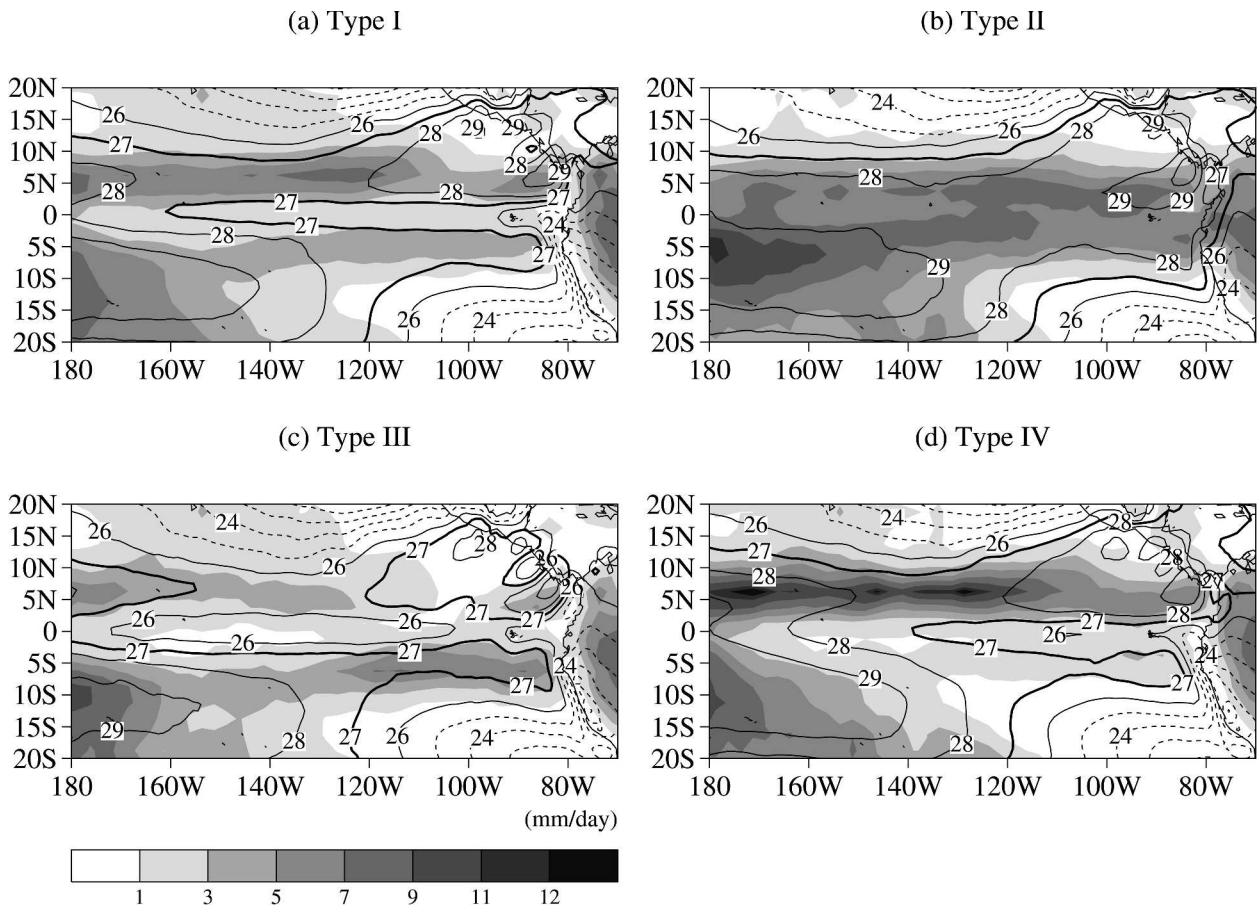


FIG. 15. Composite horizontal distributions of monthly GPCP rainfall (mm day^{-1} ; shaded) and Reynolds SST ($^{\circ}\text{C}$; contours) for the four ITCZ types during Mar–Apr.

SST maxima. At a given time, rainfall maxima are displaced meridionally from SST maxima by no more than a few degrees. To the extent the two are displaced, rainfall maxima tend to lie poleward of SST maxima. This result is different from what was previously found (Lietzke et al. 2001), and is probably due to the different datasets that were used. The surface pressure field in March and April has a broad minimum on or near the equator, with the rainfall maxima lying generally clearly poleward of the pressure minimum, which is different from what is found in other seasons.

There appears to be a competition between the two ITCZs as measured by rainfall. When one is strong, there is a tendency for the other to be weak, with the total rainfall that is integrated over both varying less than the difference between the two. In the TRMM data, a similar signal is found in the SST, suggesting that the rainfall competition is a manifestation of coupled ocean–atmosphere dynamics. In the longer-record Reynolds SST data, such a signal is much less apparent, because there is much more variability in the total SST integrated over both ITCZs. This would tend to suggest more of an independent role for atmospheric dynamics in creating the rainfall competition. Even in the TMI data there is evidence for independent atmospheric dynamics, because in April of 1999 and 2003 there are very similar SST structures but very different rainfall structures, with a strong southern ITCZ in 1999 and almost none in 2003; also, at a given rainfall value, the points along 5°S tend to correspond to lower SST and somewhat weaker surface convergence than those at 5°N.

As found previously (Liu and Xie 2002), the double convergence zone derived from the QuikScat wind field appears to be a much more frequently observed phenomenon than are the two rainfall peaks often used to quantify the ITCZs in the eastern Pacific. The double ITCZ that is defined by convection and rainfall is only observed during boreal spring, and even then monthly and weekly mean rainfall do not always follow surface convergence patterns exactly. Water vapor and cloud liquid water maxima appear when and where significant mean convective and rainfall bands are observed, qualitatively consistent with the results shown in Zhang (2001) and Lietzke et al. (2001). However, in several cases regional water vapor and cloud liquid water peaks are not associated with significant rainfall.

Many of the double-ITCZ features found in the TRMM data are confirmed by the long-record datasets from the GPCP and NCEP–NCAR reanalysis project. Four types of the ITCZs are categorized, based on the GPCP rainfall. The intense convective bands, particularly the southern ITCZ, seem to be determined not only by the local SST but also by the intensity of the equatorial cold tongue and, surprisingly, the SST north of the equator (possibly through its impact on the regional atmospheric large-scale circulation).

Acknowledgments. The authors thank Dr. Chidong Zhang for his comments and suggestions. We would also like to thank the editor, Dr. Emanuel, and two anonymous reviewers for their constructive comments and suggestions. Mr. David Bolvin prepared the TRMM and GPCP rainfall data. Both TMI products and QuikScat wind vectors were downloaded from <http://www.ssmi.com>. The NCAR–NCEP reanalysis rainfall data were kindly provided by Dr. John Janowiak. The NCAR–NCEP reanalysis surface pressure data were provided by the NOAA–CIRES Climate Diagnostics Center, in Boulder, Colorado, from its Web site online at <http://www.cdc.noaa.gov>. The NOAA OIv2 SST data were downloaded from <ftp://ftp.prd.ncep.noaa.gov/pub/cmb/sst/>. This work is supported through the TRMM Science Team under the NASA Headquarters TRMM Program Scientist Dr. Ramesh Kakar.

REFERENCES

- Adler, R. F., G. J. Huffman, D. T. Bolvin, S. Curtis, and E. J. Nelkin, 2000: Tropical rainfall distributions determined using TRMM combined with other satellite and rain gauge information. *J. Appl. Meteor.*, **39**, 2007–2023.
- , and Coauthors, 2003: The Version-2 Global Precipitation Climatology Project (GPCP) Monthly Precipitation Analysis (1979–present). *J. Hydrometeorol.*, **4**, 1147–1167.
- Bretherton, C. S., M. E. Peters, and L. E. Back, 2004: Relationships between water vapor path and precipitation over the tropical oceans. *J. Climate*, **17**, 1517–1528.
- Fu, R., A. D. Del Genio, and W. B. Rossow, 1990: Behavior of deep convective clouds in the tropical Pacific deduced from ISCCP radiance. *J. Climate*, **3**, 1129–1152.
- Gadgil, S., P. V. Joseph, and N. V. Joshi, 1984: Ocean–atmosphere coupling over monsoon regions. *Nature*, **312**, 141–143.
- Graham, N., and T. P. Barnett, 1987: Observations of sea surface temperature and convection over tropical oceans. *Science*, **238**, 657–659.
- Hack, J. J., W. H. Schubert, D. E. Stevens, and H. Kuo, 1989: Response of the Hadley circulation to convective forcing in the ITCZ. *J. Atmos. Sci.*, **46**, 2957–2973.
- Halpern, D., and C.-W. Hung, 2001: Satellite observations of the southeast Pacific intertropical convergence zone during 1993–1998. *J. Geophys. Res.*, **106**, 28 107–28 112.
- Hayes, S. P., M. J. McPhaden, and J. M. Wallace, 1989: The influence of sea-surface temperature on surface wind in the eastern equatorial Pacific: Weekly to monthly variability. *J. Climate*, **2**, 1500–1506.
- Held, I. M., and B. J. Soden, 2000: Water vapor feedback and global warming. *Annu. Rev. Energy Environ.*, **25**, 441–475.
- Hubert, L. F., A. F. Krueger, and J. S. Winston, 1969: The double Intertropical Convergence Zone—Fact or fiction? *J. Atmos. Sci.*, **26**, 771–773.
- Hurrell, J. W., and K. E. Trenberth, 1998: Difficulties in obtaining reliable temperature trends: Reconciling the surface and satellite microwave sounding unit records. *J. Climate*, **11**, 945–967.
- Johnson, R. H., T. M. Rickenbach, S. A. Rutledge, P. E. Ciesielski, and W. H. Schubert, 1999: Trimodal characteristics of tropical convection. *J. Climate*, **12**, 2397–2418.
- Kalnay, E., and Coauthors, 1996: The NCEP/NCAR 40-Year Reanalysis Project. *Bull. Amer. Meteor. Soc.*, **77**, 437–471.
- Kessler, W. S., L. M. Rothstein, and D. Chen, 1998: The annual cycle of SST in the eastern tropical Pacific, diagnosed in an ocean GCM. *J. Climate*, **11**, 777–799.

- Li, T., and S. G. Philander, 1996: On the annual cycle of the eastern equatorial Pacific. *J. Climate*, **9**, 2986–2998.
- Lietzke, C. E., C. Deser, and T. H. Vonder Haar, 2001: Evolutionary structure of the eastern Pacific double ITCZ based on satellite moisture profile retrievals. *J. Climate*, **14**, 743–751.
- Liu, W. T., and X. Xie, 2002: Double intertropical convergence zones—A new look using scatterometer. *Geophys. Res. Lett.*, **29**, 2072, doi:10.1029/2002GL015431.
- , W. Tang, and P. S. Polito, 1998: NASA scatterometer provides global ocean-surface wind fields with more structures than numerical weather prediction. *Geophys. Res. Lett.*, **25**, 761–764.
- Mechoso, C. R., and Coauthors, 1995: The seasonal cycle over the tropical Pacific in coupled ocean–atmosphere general circulation models. *Mon. Wea. Rev.*, **123**, 2825–2838.
- Mitchell, T. P., and J. M. Wallace, 1992: The annual cycle in equatorial convection and sea surface temperature. *J. Climate*, **5**, 1140–1156.
- Neelin, J. D., C. Chou, and H. Su, 2003: Tropical drought regions in global warming and El Niño teleconnections. *Geophys. Res. Lett.*, **30**, 2275, doi:10.1029/2003GLO018625.
- Philander, S. G. H., D. Gu, G. Lambert, T. Li, D. Halpern, N.-C. Lau, and R. C. Pacanowski, 1996: Why the ITCZ is mostly north of the equator. *J. Climate*, **9**, 2958–2972.
- Reynolds, R. W., N. A. Rayner, T. M. Smith, D. C. Stokes, and W. Wang, 2002: An improved in situ and satellite SST analysis for climate. *J. Climate*, **15**, 1609–1625.
- Sobel, A. H., I. M. Held, and C. S. Bretherton, 2002: The ENSO signal in tropical tropospheric temperature. *J. Climate*, **15**, 2702–2706.
- Soden, B. J., 2000: The sensitivity of the tropical hydrological cycle to ENSO. *J. Climate*, **13**, 538–549.
- Su, H., and J. D. Neelin, 2003: The scatter in tropical average precipitation anomalies. *J. Climate*, **16**, 3966–3977.
- Tomas, R. A., and P. J. Webster, 1997: The role of inertial instability in determining the location and strength of near-equatorial convection. *Quart. J. Roy. Meteor. Soc.*, **123**, 1445–1482.
- Wentz, F. J., 1997: A well-calibrated ocean algorithm for special sensor microwave/imager. *J. Geophys. Res.*, **102**, 8703–8718.
- , and M. Schabel, 2000: Precise climate monitoring using complementary satellite data sets. *Nature*, **403**, 414–416.
- Zhang, C., 2001: Double ITCZs. *J. Geophys. Res.*, **106**, 11 785–11 792.
- , M. McGauley, and N. A. Bond, 2004: Shallow meridional circulation in the tropical eastern Pacific. *J. Climate*, **17**, 133–139.
- Zheng, Q., X.-H. Yan, W. T. Liu, W. Tang, and D. Kurz, 1997: Seasonal and interannual variability of atmospheric convergence zones in the tropical Pacific observed with ERS-1 scatterometer. *Geophys. Res. Lett.*, **24**, 261–263.